ADVANCED MATERIALS
www.advmat.de

Strain-Driven Negative Resistance Switching of Conductive Fibers with Adjustable Sensitivity for Wearable Healthcare Monitoring Systems with Near-Zero Standby Power

Won Kyung Min, Chihyeong Won, Dong Hyun Kim, Sanghyeon Lee, Jusung Chung, Sungjoon Cho, Taeyoon Lee, and Hyun Jae Kim**

Recently, one of the primary concerns in e-textile-based healthcare monitoring systems for chronic illness patients has been reducing wasted power consumption, as the system should be always-on to capture diverse biochemical and physiological characteristics. However, the general conductive fibers, a major component of the existing wearable monitoring systems, have a positive gauge-factor (GF) that increases electrical resistance when stretched, so that the systems have no choice but to consume power continuously. Herein, a twisted conductive-fiber-based negatively responsive switch-type (NRS) strain-sensor with an extremely high negative GF (resistance change ratio $\approx 3.9 \times 10^8$) that can significantly increase its conductivity from insulating to conducting properties is developed. To this end, a precision cracking technology is devised, which could induce a difference in the Young's modulus of the encapsulated layer on the fiber through selective ultraviolet-irradiation treatment. Owing to this technology, the NRS strain-sensors can allow for effective regulation of the mutual contact resistance under tensile strain while maintaining superior durability for over 5000 stretching cycles. For further practical demonstrations, three healthcare monitoring systems (E-fitness pants, smart-masks, and posture correction T-shirts) with near-zero standby power are also developed, which opens up advancements in electronic textiles by expanding the utilization range of fiber strain-sensors.

1. Introduction

Over the past decades, the telemedicine market has been rapidly expanding worldwide, and the focus of the market is shifting from "the diagnosis and treatment of diseases" to "the prevention of disease and healthcare management in daily life".[1] These trends have occurred while digital technology has been driving a revolution in healthcare, or so-called "digital healthcare," which spans a wide range of uses from mobile medical apps to software that support clinical decisions doctors make every day.[2] In particular, patients with chronic diseases, such as high blood-pressure, diabetes, respiratory diseases, and disc diseases, who must always manage their health, could benefit the most from this.[3] For them, daily wearable monitoring systems attached to or worn on the body are essential to identify early warning signs using biometric data, such as pulse, blood pressure, body strain, and the motions of the joints, captured from wearable digital healthcare devices with customized services.[4] However, although these wearable devices should pick up vital signals of the user's health in real-time while minimizing discomfort, most popular wearable devices on the market are still limited to wrist types in the form of rigid accessories due to the restrictions of the materials used to construct the electronic devices.[5,6] To overcome this issue, textile-based electronics are highly anticipated as one of the representative next-generation wearable devices for monitoring systems that can be applied to various parts of our bodies while having superior elasticity.[7–11]

W. K. Min, D. H. Kim, H. J. Kim
Electronic Device Laboratory
School of Electrical and Electronic Engineering
Yonsei University
50 Yonsei-ro, Seodaemun-gu, Seoul 03722, Republic of Korea
E-mail: hjk3@yonsei.ac.kr

C. Won, S. Cho, T. Lee
Nanobio Device Laboratory
School of Electrical and Electronic Engineering
Yonsei University
50 Yonsei-ro, Seodaemun-gu, Seoul 03722, Republic of Korea
E-mail: taeyoon.lee@yonsei.ac.kr

S. Lee
KIURI Institute
Yonsei University
50 Yonsei-ro, Seodaemun-gu, Seoul 03722, Republic of Korea

J. Chung
BIT Micro Fab Research Center
Yonsei University
50 Yonsei-ro, Seodaemun-gu, Seoul 03722, Republic of Korea

The ORCID identification number(s) for the author(s) of this article can be found under https://doi.org/10.1002/adma.202303556

DOI: 10.1002/adma.202303556

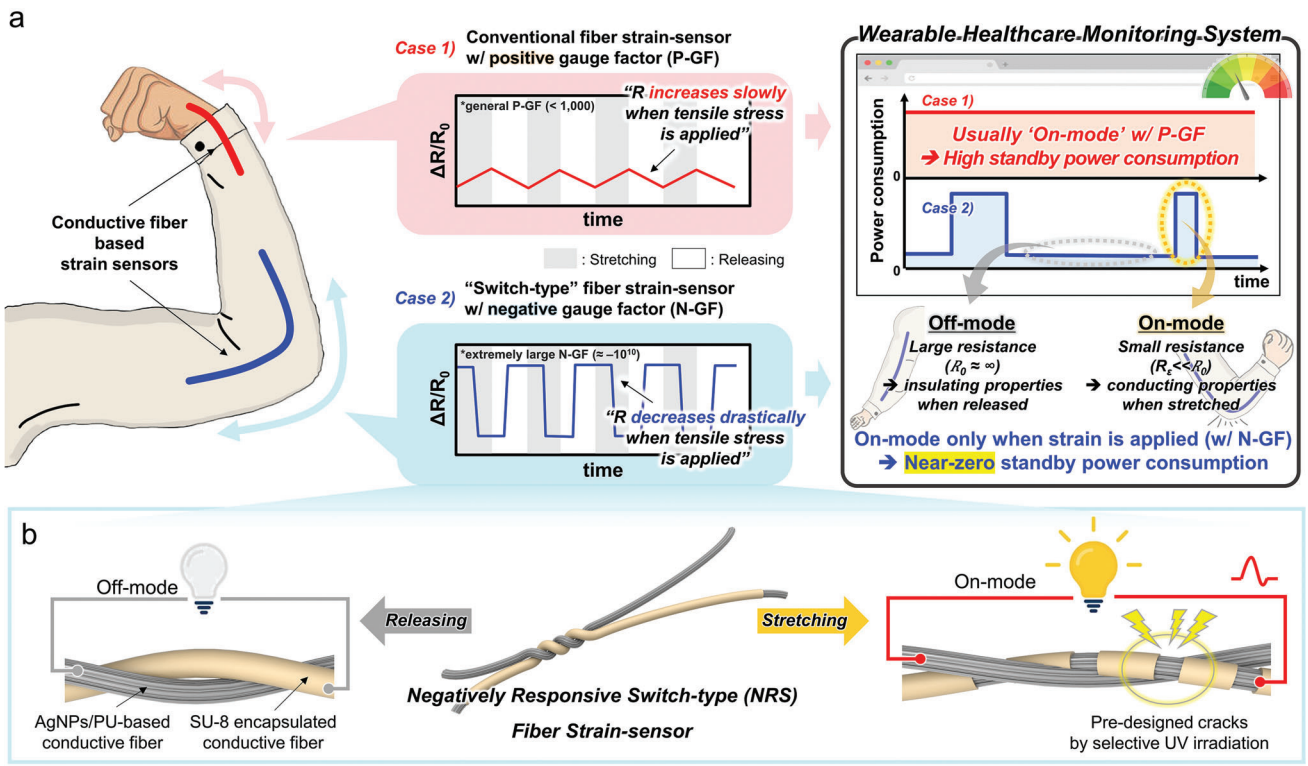

Figure 1. The necessity for a strain-sensor with N-GF characteristics in the textile-based monitoring systems with our conception of the developed strain-sensors. a) An exemplary schematic illustration of conductive-fiber-based strain-sensors with P-GF or N-GF characteristics and wearable healthcare monitoring systems using them. b) Conceptual schematic illustration of the negatively responsive switch-type (NRS) strain-sensor.

As a vital component of textile-based wearable monitoring systems, stretchable conductive-fiber-based strain-sensors have been widely employed because they can be easily woven into diverse clothing and can convert physical deformations generated by human's physiological activities and various body movements into measurable signals.[12–17] However, the existing conductive-fiber-based strain-sensors are disadvantageous in terms of power consumption for the wearable monitoring systems because typical conductive fibers usually detect tensile strain through increased resistance, which is expressed as a positive gauge factor (P-GF).[18–22] At this point, it can maintain a low resistance value of ≈1000 Ω or less to continuously transmit signals to the system, resulting in continuous high-power consumption even throughout the long standby time where no deformation has occurred.[18,19,23] In an effort to address the power consumption issue, some researchers have explored the use of piezoelectric materials to develop self-powered fiber sensors.[24] However, most piezoelectric materials, such as $BaTiO_3$ or PZT ($PbZr_xTi_{1-x}O_3$), present challenges for textile-based strain-sensor fabrication due to their complex deposition methods as well as their relatively rigid and fragile nature under strain.[25,26] As a result, these materials are more inclined toward flexible and bendable applications, such as pressure sensors, rather than truly stretchable ones, potentially limiting their use in wearable, and textile devices designed for the human body. Thus, there is still a pressing need for novel approaches to efficiently resolve the energy consumption problem in real-time monitoring devices.

To reduce the power consumption of always-on wearable monitoring systems, however, conductive fibers with a negative gauge factor (N-GF) are desirable because they can be used to control standby power consumption.[27–29] In general, because the standby time is relatively longer than the operating time, reducing standby power consumption is a core strategic step for implementing low-power monitoring systems. For a detailed explanation of how the conductive fiber with N-GF can reduce this standby power, two example fiber strain-sensors with general P-GF (<1000) and extremely high N-GF (≈-10^{10}) are compared in **Figure 1**a. If conventional fiber strain-sensors with general P-GF are used in monitoring systems, the system will operate in the "on-mode" most of the time even when no strain is applied, resulting in high power consumption. Consequently, their increased resistance upon stretching renders them unsuitable for use as interconnects between other biosensors in systems that operate only when stretched, as this increase interrupts the connection. However, if fiber strain-sensors with extremely high N-GF (labeled as "switch-type") are used, the system cannot operate in a normal released state, but the current through the system can flow only when strain occurs; thus, the standby power consumption could be near-zero because the system is turned on only under specific circumstances. In other words, if the resistive characteristics of these switch-type strain-sensors could change from insulating to conducting properties only when stretched, their large resistance ($R_0 \cong \infty$) without strain would operate in the "off-mode", while a small resistance under strain

($R_\varepsilon << R_0$) would allow for real-time detection and operate in the "on-mode". Therefore, they could function as a mechano-electric switch that operates as a strain as a gate, and might be used to implement a strain-responsive interconnect for the monitoring system that transmits biological signals only when triggered by an abnormally functioning body or by the applied strain.[30]

To date, negatively stretching–resistive switch-type conductive fibers, which can effectively regulate the power consumption of the monitoring systems, have rarely been developed.[31,32] According to state-of-the-art reports about fiber-based strain-sensors (Table S1, Supporting Information), the GF values in most of these studies are positive; consequently, these devices have a finite resistance even in the absence of strain and are unsuitable for low-power standby applications.[18] In addition, some textiles in which conductive fibers are woven into knots with N-GF have been rarely reported,[28,33,34] but they are already highly conductive before stretching and exhibit a poor on/off ratio (<10). This limits their applicability in highly deformable textile electronics intended for use in low-power wearable monitoring systems with near-zero standby power. Furthermore, to integrate them into wearable healthcare monitoring systems, conductive fibers with N-GF that can precisely control the sensitivity of each body part according to different strain levels are required, but no approach has yet been developed.

Here, we developed a negatively responsive switch-type (NRS) fiber strain-sensor that allows for adjustable sensitivity through pre-designed crack localizing technologies. This was accomplished by leveraging the existing fiber sensor fabrication process[35,36] and incorporating a novel structural modification, which involved twisting two different fibers to enhance durability and conformability across various surfaces and simultaneously achieve an extremely high N-GF, essential for low-power standby applications. As shown in Figure 1b, the twisted fibers comprise an Ag nanoparticle (AgNP)/polyurethane (PU)-based conductive fiber and another fiber encapsulated with a crack-controlled insulating thin film on it. Specifically, they are intended to contact each other delicately between the strain-generated cracks and boost their mutual conductivity only when they are stretched. To arrange cracks in the insulator layer as desired, SU-8, which is commonly used as a photoresist, was chosen for the insulator layer, and the generation of cracks was accurately controlled by inducing a Young's modulus difference by selective ultraviolet (UV)-irradiation treatment. Then, by controlling the number of times the fibers were twisted and thereby localizing the pre-generated cracks, a wide range of strain-sensors with varying sensitivities to different strain strengths could be fabricated. As a visual demonstration of this one-of-a-kind performance, such sensors been applied to fabric-based stretchable LED arrays with hidden-pixels that function only when stretched. In a further step, we validated their practical applicability by integrating them into simple wearable healthcare monitoring systems that are activated only when the user wears them or in problematic situations. This points to a new possibility of negatively strain-resistive conductive fibers enabling a long lifetime of monitoring systems by consuming near-zero standby power.

2. Results and Discussion

2.1. Fabrication of Single Conductive Fibers with Crack-Controlled Insulator Encapsulation

To fabricate twisted conductive-fiber-based NRS strain-sensors with the aforementioned N-GF switching properties, two prerequisites are required. First, an insulating barrier is necessary to prevent mutual currents from flowing between the two conductive fibers before stretching them. Second, the size and density of the cracks generated by tensile strain in the thin insulating barrier should be freely adjustable so that the current can flow to the two fibers at the desired tensile strain strength. To achieve them, we developed a strategy to prepare an encapsulation structure with SU-8 photoresist as the insulating barrier, whose degree of curing varies depending on post-treatment methods through UV-irradiation (wavelength of 185 and 254 nm).[37] **Figure 2**a shows a scheme of the fabrication process for the conductive fiber encapsulated in a crack-controlled SU-8 insulating layer. An AgNP/PU-based conductive fiber with highly stretchable and conductive properties was prepared through a reduction process of an Ag precursor for even distribution of Ag nanoparticles on its surface in a well-established manner (see the Experimental Section for details). As in previously published papers,[12] these fibers are composed of multifilament to maintain their superior conductivity even when stretched. Actually, the precise term for these sensors should be "multifilament fiber strain-sensors" or "yarn strain-sensors". However, in order to maintain consistency with previous research, we have chosen to refer to them as "fiber strain-sensors". The SU-8 encapsulation layer is then deposited on the conductive fibers using the dip-coating method, except for both ends that should maintain conductivity. Subsequently, pre-baking at 85 °C for 10 min is carried out, and the manufactured fiber is selectively UV-irradiated for 2 h with a shadow mask comprising repeated stripes. For this experiment, we designed and fabricated a customized flexible shadow mask, as shown in Figure S1 (Supporting Information), tailored to the fiber's cylindrical shape to ensure optimal light transmission and minimal diffraction during the UV curing process. A cross-sectional scanning electron microscopy (SEM) image of the encapsulated fiber and its energy-dispersive X-ray spectroscopy (EDS) were measured, as shown in Figure 2b and Figure S2 (Supporting Information), respectively. Thus, the SU-8 encapsulation layer was uniformly well-coated all around the multifilament-structured conductive fiber, forming a nearly perfect cylindrical shape with a diameter of ≈580 μm.

To determine how the cracks form when the SU-8 encapsulated conductive fibers are stretched, the SEM images depicted in Figure 2c were analyzed and compared before and after 20% tensile strain. Surprisingly, depending on how UV-irradiation is carried out, the shape of the cracks that are generated during stretching dramatically changes. If the encapsulated fiber in the non-irradiated SU-8 encapsulation layer is stretched, striped shapes in the direction of the tensile strain were generated on the encapsulation layer, as opposed to the formation of cracks or breaks. This indicates that the encapsulation layer has been stretched to some degree as a result of an insufficient curing step. However, when UV-irradiation was performed on the overall encapsulation layer,

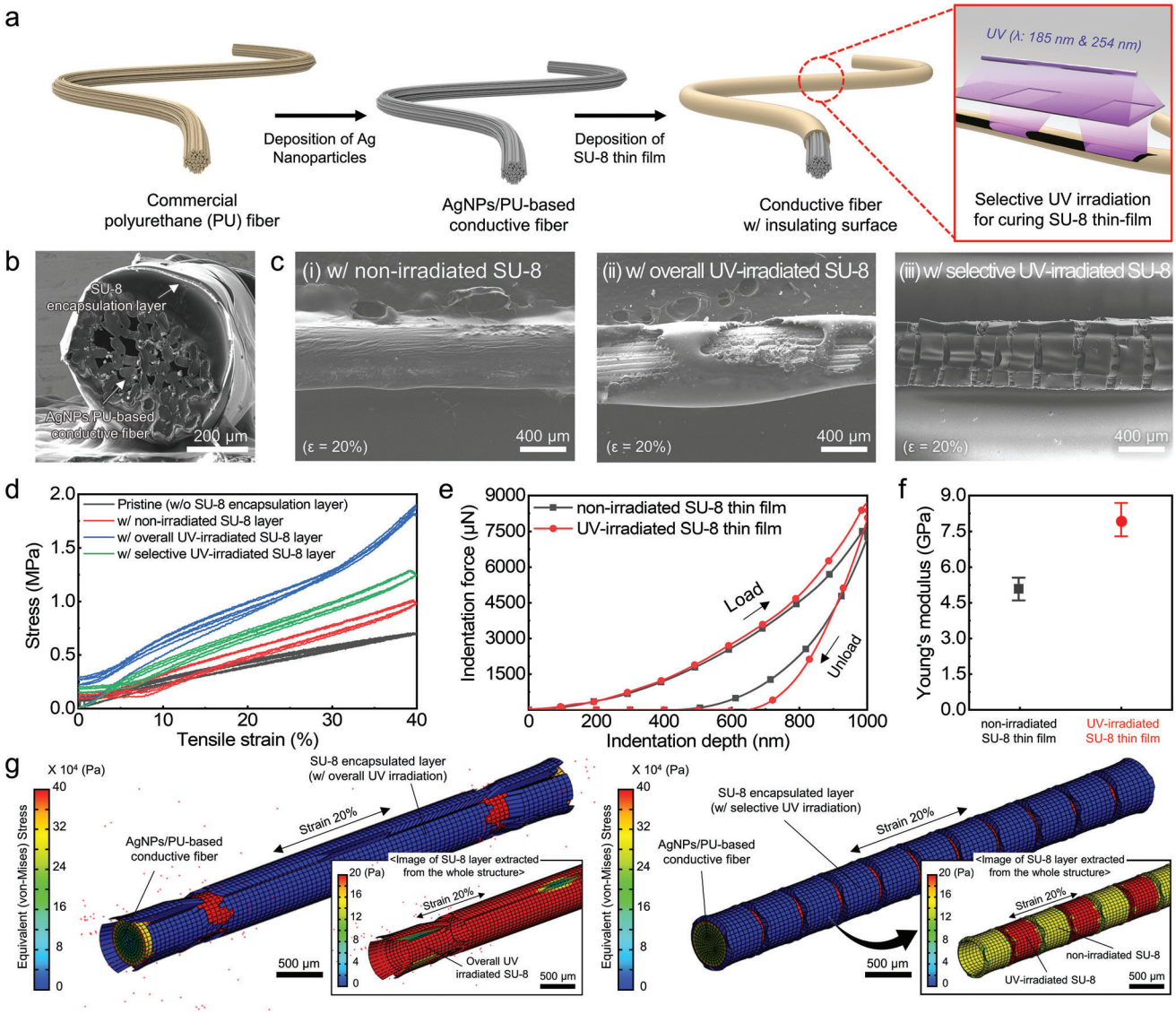

Figure 2. Fabrication and characterization of the SU-8 encapsulated single conductive fiber. a) Schematic illustration of the fabrication process for the single conductive fiber. b) A cross-sectional SEM image of the single conductive fiber. c) Typical SEM images showing the surface of the SU-8 encapsulation layer with different UV-irradiation post-treatment with a non-irradiated SU-8 layer (i), with an overall UV-irradiated SU-8 layer (ii), and with a selective UV-irradiated SU-8 layer (iii) after 20% tensile strain. d) Stress–strain curves of the single conductive fibers with and without SU-8 encapsulation layer. e) Loading–unloading curves of non-irradiated and UV-irradiated SU-8 thin films with varying indentations force by nanoindentation methods. f) Young's modulus of non-irradiated and UV-irradiated SU-8 thin films (statistical data of five samples). g) FEM simulation analysis of the single conductive fibers with overall and selective UV-irradiated SU-8 layer in 20% stretched modes.

cracks were arbitrarily generated, exposing the conductive fibers within because the encapsulation layer was too hardened to be stretched. Nonetheless, it can be observed that these cracks were extremely non-uniform and had a random size distribution.

To take advantage of the fact that the crack formation characteristics vary depending on the presence or absence of UV-irradiation, selective UV-irradiation treatment was applied alternatively to ≈50% of the area using a shadow mask with a repeated 300 μm-wide stripe. Thus, clearly, cracks occurred only at the boundary between the UV-irradiated area and the non-irradiated area, and those cracks were generated uniformly with a very uniform size of ≈300 μm, comparable to the size of the shadow mask stripes. Furthermore, by varying the stripe width of the shadow mask from 100 to 500 μm, the effect of this selective UV treatment can be verified by comparing the size of cracks under 20% tensile strain after UV treatment (Figure S3, Supporting Information). This change in the crack formation was also indirectly confirmed through three repeated stress–strain curves for the fabricated fibers, as shown in Figure 2d. The hysteresis and slight plastic deformation of the fibers can be attributed to the time-dependent behavior and stress relaxation of free chains in the network of the viscoelastic elastomer in the fibers.[12,38] In subsequent stretching, all conductive fibers exhibited negligible hysteresis even after three repeated stretching–releasing cycles;

however, the magnitude of stress according to strain varied considerably. This allowed us to confirm that strain-induced stress can be reduced by ≈40% if UV treatment is performed selectively as opposed to overall treatment. This phenomenon could be attributed to the formation of uniform cracks, which permit the fiber to be stretched more easily, even when encapsulated in a rigid material.

To analyze the cause of changes in crack formation according to UV-irradiation methods, we performed nanoindentation analysis and finite element analysis (FEA) simulations for UV-irradiated and non-irradiated SU-8 thin films. Figure 2e shows the nanoindentation results of the loading–unloading curve, and Figure 2f depicts the statistical Young's modulus data for five measurements with different regions in the two films. The UV-irradiated SU-8 thin film exhibited a high Young's modulus (8.2 ± 0.8 GPa), whereas the non-irradiated SU-8 thin film exhibited a lower Young's modulus (5.1 ± 0.4 GPa). Through this, we found that when the SU-8 thin film was UV-irradiated, the degree of curing differed from that of the non-irradiated thin film, so that the degree of deformation during stretching could be reduced by almost 1.6 times. In addition, FEA simulations were performed using the explicit dynamics module of the ANSYS workbench computational simulation tool to further understand how the difference in Young's moduli affects crack distribution. Figure 2g shows the result of analyzing the equivalent (von Mises) stress applied to each layer at 20% tensile strain using the previously measured physical property information. While the stretchable fibers are subjected to a maximum stress of ≈38 000 Pa, each SU-8 encapsulation layer has already generated cracks and thus suffers little deformation stress; however, the shape of crack formation varies considerably depending on UV-treatment conditions. Upon closer inspection, we confirmed that the overall UV-irradiated SU-8 encapsulation layer was fractured at both ends after 20% tensile strain, thereby forming disordered and non-uniform cracks. In contrast, when the physical property information of the UV-irradiated SU-8 encapsulation layer and the non-irradiated SU-8 encapsulation layer was alternately applied to the encapsulation layer at every 500 μm, regular and uniform cracks were generated only at the interface. These results can also be observed in the inset image, in which only the SU-8 encapsulation layer has been extracted; this result corresponds to the crack shapes observed in the preceding SEM images. Thus, it could be assumed that the size and density of the cracks in the SU-8 encapsulation layer could be controlled as desired by using the difference in the Young's moduli between the UV-irradiated region and the non-irradiated region interface through this selective UV-irradiation treatment.

This mechanism is similar to the "rigid-islands" concept recently studied and utilized by researchers in stretchable electronics and displays to effectively alleviate strain stress.[6,39,40] The rigid islands are strategically placed, non-deformable regions in a stretchable device, designed to preserve the performance of electronic components, such as transistors, sensors, and other circuit elements. They protect these components from excessive strain that could potentially damage their delicate structures or compromise their electrical properties. In our NRS fiber strain-sensor, the SU-8 encapsulation layer with selectively opened cracks functions similarly to these rigid-islands, enabling the sensor to withstand strain without delamination from the PU-based stretchable fiber. This effective stress management of the SU-8 encapsulation layer, allowing it to function without mechanical delamination while maintaining cracks after 100 stretching and releasing cycles, can be observed in the SEM image in Figure S4 (Supporting Information).

2.2. Fabrication and Characterization of Twisted Fiber-Based Negatively Responsive Switch-Type (NRS) Strain-Sensors

Figure 3a depicts a schematic diagram of the fabricated NRS strain-sensor comprising two conductive fibers double-twisted to one another at their central point of contact before and after stretching. Specifically, one of the twisted conductive fibers is encapsulated with the crack-controlled insulating layer described in the preceding section. This structure is designed to secure N-GF characteristics, and the drastic resistance change mechanism according to the strain we predicted is as follows. Before stretching, cracks are not generated in the insulating encapsulation layer; thus, the conductive fiber and the insulator-encapsulated fiber come into contact, preventing the current flow due to their high mutual resistance. In other words, the contact resistance (R_C), which represents the resistance between two adjacent conductive fibers in the vertical direction, is almost infinitely large, and the twisted fibers are in an open-circuit state. However, upon stretching, the two adjacent fibers perpendicular to the tensile stress become more and more compact with increasing strain and become closer accordingly. At this time, uniform cracks are induced in the rigid insulating encapsulation layer, and the exposed conductive fiber regions between the generated cracks come into contact with each other, significantly reducing their mutual resistance, including R_C, and allowing current to flow.

To implement this mechanism of the NRS fiber strain-sensors in practice, we fabricated a device by twisting both the AgNP/PU-based conductive fiber and the fiber encapsulated with the SU-8 insulating thin film, as shown in Figure 3b. Thus, as shown in Figure 3c, which depicts the SEM image of the device before and after 20% stretching, the two conductive fibers do not contact each other prior to stretching because there is no crack in the SU-8 layer; however, after stretching, the two conductive fibers could contact each other between the uniformly generated cracks. Subsequently, two different types of resistance changes are measured to analyze whether they could induce a change in the gauge factor according to the aforementioned mechanism: single resistance and mutual resistance. Figure 3d shows the measured single and mutual resistive properties according to the strain of the pristine conductive fiber without the encapsulation layer, the fiber with the SU-8 encapsulation layer, and the twisted fibers. The initial single resistances of the fibers with and without the SU-8 encapsulation layer were 15.6 and 14.0 Ω, respectively. The resistance of the pristine fiber increased with tensile strain, exhibiting a P-GF of 143.5, and it lost electrical conduction at ≈100% tensile strain. The resistance of the conductive fiber encapsulated with SU-8 showed a similar tendency, but it rapidly increased with the tensile strain exhibiting a relatively higher P-GF of 181.1, and the maximum tensile range maintaining the low resistance (<1000 Ω) was slightly reduced. Here, the change in single resistance was derived from the reversible percolation network with

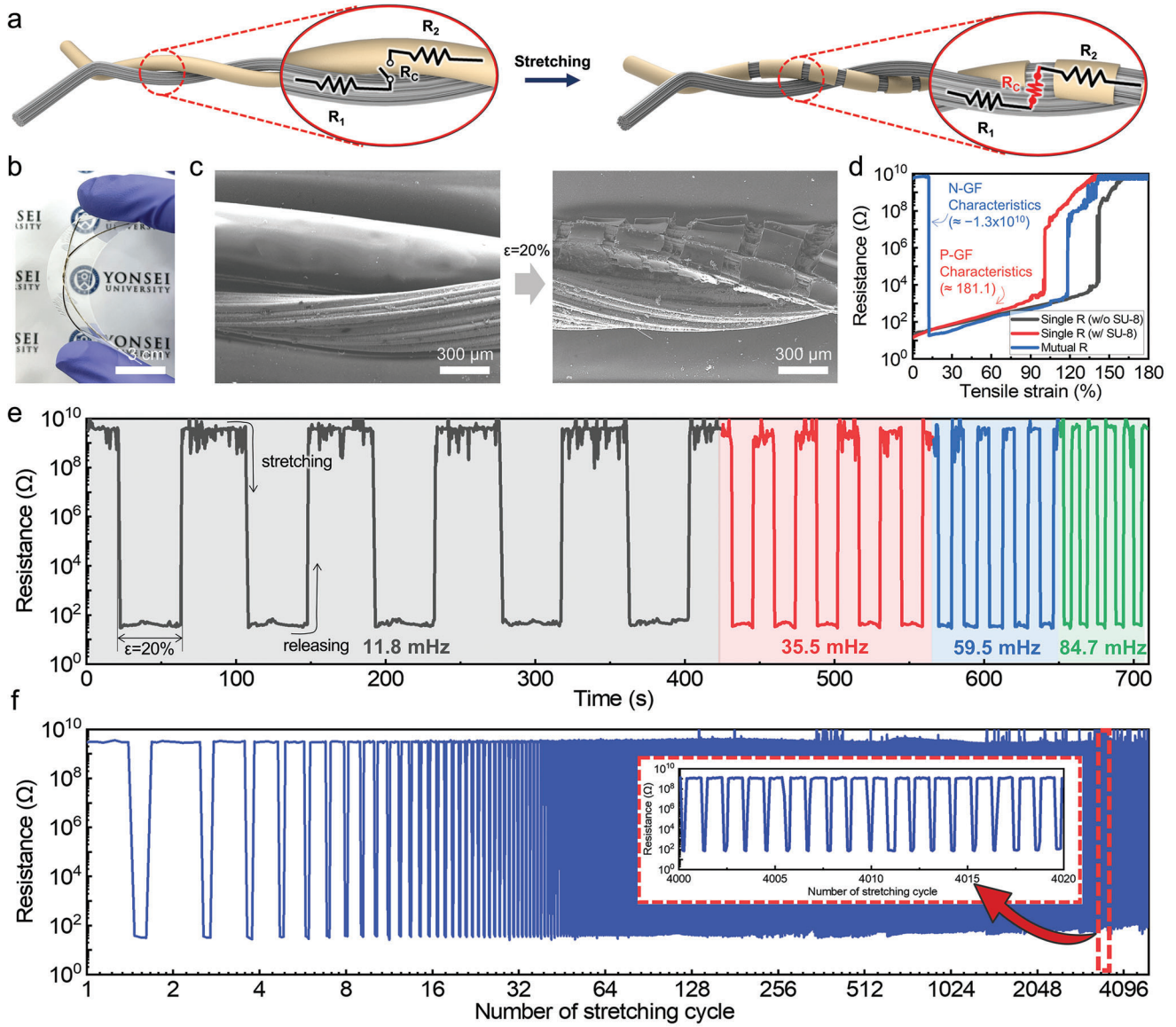

Figure 3. Overall strain-sensing performance of the twisted-fiber based NRS strain-sensors. a) Schematic illustrations depicting the structure and resistance model of the NRS fiber strain-sensors before and after stretching. b) Photographic image of the fabricated NRS fiber strain-sensor. c) Typical SEM images showing the fabricated NRS fiber strain-sensors before and after 20% stretching. d) Single and mutual electrical resistance characteristics of the NRS fiber strain-sensors as a function of the initially applied maximal strain. e) Electrical resistance variation under cyclic stretching–releasing with a strain of 20% at frequency of 11.8, 35.5, 59.5, and 84.7 mHz. f) Performance of the NRS fiber strain-sensor under 5000 stretching–releasing cycles of strain variation from 0 to 20%, with an inset of the magnified cycles from the marked box.

the distribution of microcracks throughout the single conductive fiber upon applied strains, as reported in previous research.[41]

However, the mutual resistance of the twisted fibers is considerably reduced in response to the lateral tensile strain. Up to ≈14% tensile strain, the mutual resistance is $\approx 10^{10}$ Ω, but as this is the limit of the measuring equipment, it can be concluded that there is no contact with each other at all. Then, the mutual resistance hardly changes up to 12%, then rapidly decreases to 18 Ω at tensile strain in the range of 12.2% to 12.4%, indicating -6.5×10^{11} of N-GF characteristics. Subsequently, the resistance gradually increases, showing similar characteristics to the previous single fibers. It might be assumed that these negatively strain-resistive switching properties originate from the numerous contacts between the generated cracks in the SU-8 insulating layer contacts of two twisted conductive fibers, as shown by previous SEM image analysis. In relation to the dramatical contact resistance changes caused by the "open and close" of these cracks, a detailed dynamic model of the resistance changes in the NRS fiber strain-sensor during stretching could be found in Figures S5–S9 (Supporting Information).

Figure 3e displays the relative resistance variation under cyclic stretching–releasing with a tensile strain of 20% at speed frequencies of 11.8, 35.5, 59.5, and 84.7 mHz. Similar to the above results, these devices exhibited negative strain-resistive switch-

ing characteristics with a response time of 565.25 ms and a resistive switching on/off ratio of $\approx 10^8$ for every five cycles. The performances of the fabricated NRS fiber strain-sensors were almost independent of the frequency within the tested range (11.8–84.7 mHz), implying the excellent stability of the sensor under different frequencies. Additionally, as shown in Figure S10 (Supporting Information), even when stretched up to 100%, it was observed that the negative switching response could be maintained at a specific threshold tensile strain.

Moving forward, the durability of the NRS strain-sensor was intensively investigated through repetitive stretching cycles, as shown in Figure 3f. The resistance values of the strain-sensor exhibited a slight increase due to the viscoelastic properties of the elastomeric fiber; however, these resistance change characteristics remained stably maintained without considerable degradation throughout the intensive 5000 cycle tests with 20% tensile strain, indicating its remarkable repeatability. Moreover, as evidenced in Figure S11 (Supporting Information), the performance of our strain-sensors remained consistent even after six months, highlighting their superior long-term stability in ambient conditions.

To further assess the applicability of our NRS fiber strain-sensors in various textile electronics, we conducted additional stability-related experiments. Textile electronics necessitate specific characteristics, such as mechanical durability, biocompatibility, and resistance to moisture, to ensure comfort and sustained functionality during the user's various wearing conditions. In order to address these requirements, we developed a novel passivation layer using electrospun PU nanofibers. As seen in Figure S12 (Supporting Information), this passivation layer was fabricated through a process of electrospinning ultrathin PU fibers directly onto the twisted NRS fiber strain-sensors (see the Experimental Section for details). This approach allowed the sensor to maintain its original shape under various tensile strains while isolating it from the external environment and preserving its electrical performance. Additionally, the passivation layer prevents direct skin contact with the sensor's materials, enhancing their biocompatibility for a wide range of wearable applications such as health monitoring, fitness tracking, and smart clothing. Furthermore, the NRS fiber strain-sensors maintain their performance even in washing and moist environments, as demonstrated in Figure S13 (Supporting Information). Detailed washing test results can be found in the Supporting Information. Consequently, our NRS fiber strain-sensors exhibit exceptional durability, stability, and versatility, making them a promising candidate for various applications in the rapidly evolving field of textile electronics.

2.3. Stretchable LED Arrays with a Hidden-Pixel Concept Implementing the Fabricated NRS Fiber Strain-Sensors with Adjustable Sensitivity

For the numerous applications, it is essential to develop various methods to control the strain-sensitivity (the degree of tensile strain (%) that causes resistance change). One of the representative methods for adjusting strain-sensitivity involves controlling the thickness of the fibers. As demonstrated in Figure S14 (Supporting Information), we compared the NRS fiber strain-sensors fabricated from fibers with diameters of 500 and 300 μm. Both fibers exhibited similar P-GF characteristics in single fiber (Figure S14a, Supporting Information), with resistance linearly increasing with tensile strain. As illustrated in Figure S14b–e (Supporting Information), we evaluated the performance of both NRS fiber strain-sensors, revealing that their properties were well preserved, regardless of the fiber diameter, as evidenced by the resistance change during a series of five 20% strain repetitions. However, we observed that the 300 μm diameter NRS fiber strain-sensors could exhibit a higher sensitivity, responding at ≈8% tensile strain, compared to the thicker fibers. As explained by the previously mentioned dynamic model, these differences primarily result from thinner fibers being more susceptible to contact between the twisted fibers in the presence of cracks and thus having a lower critical strain.

Besides controlling fiber thickness, we also sought to fine-tune the sensitivity using the same fabrication process by altering the number of twists to effectively regulate contact resistance. **Figure 4**a–c shows how the strain-resistive sensitivity of the fabricated NRS fiber strain-sensors varies as the number of twists is gradually increased to single, double, and triple. We increased the number of twists by fixing one end of the two fibers, rotating the other end by 180°, 360°, and 540°, and then fixing it again. To analyze the minimum tensile strain level to which each sensor responds, five cyclic stretching–releasing tests were conducted while gradually increasing the tensile strain up to 40%. It was confirmed that the single-twisted device hardly reacts to stretching up to 20% tensile strain, and that at 28% tensile strain, the resistance changes from insulator-like (6.2×10^9 Ω) to metal-like (90.4 Ω). Furthermore, these results were secured stably up to 40%. In contrast, the resistive change characteristics with a considerable reduction occurred at a lower tensile strain of 16% for double-twist devices and 8% for triple-twist devices, indicating that the sensitivity increased as the number of twists increased. These properties could also be validated by comparing the test results for the same maximum tensile strain range. For example, if we compare the respective test results in the purple region of Figure 4a–c that stretches up to 28%, the triple-twisted device responds with an 8% tensile strain before reaching the maximum tensile range of 28%, whereas the single-twisted device does not respond until the tensile strain reaches almost 28%. Consequently, for the same stretching test, a device with more twists exhibits metal-like properties for a longer period due to its high sensitivity. Meanwhile, no discernible difference was observed in the resistance value itself depending on the number of twists, and their switching characteristics remained identical at 10^8 or higher.

To determine the cause of the changes in sensitivity depending on the number of twists, which physical factors influence the contact resistance between the two general conductive fibers must be understood. As mentioned previously, the main sensing mechanism is based on the structure-induced "contact resistance" by the "open and close" effects using pre-designed cracks during the stretching and releasing cycle of the fiber. According to Holm theory,[42] for two bodies in contact, the contact resistance can be expressed using Equation (1)

$$R_c = \frac{\rho}{2}\sqrt{\frac{\pi H}{nP}} \tag{1}$$

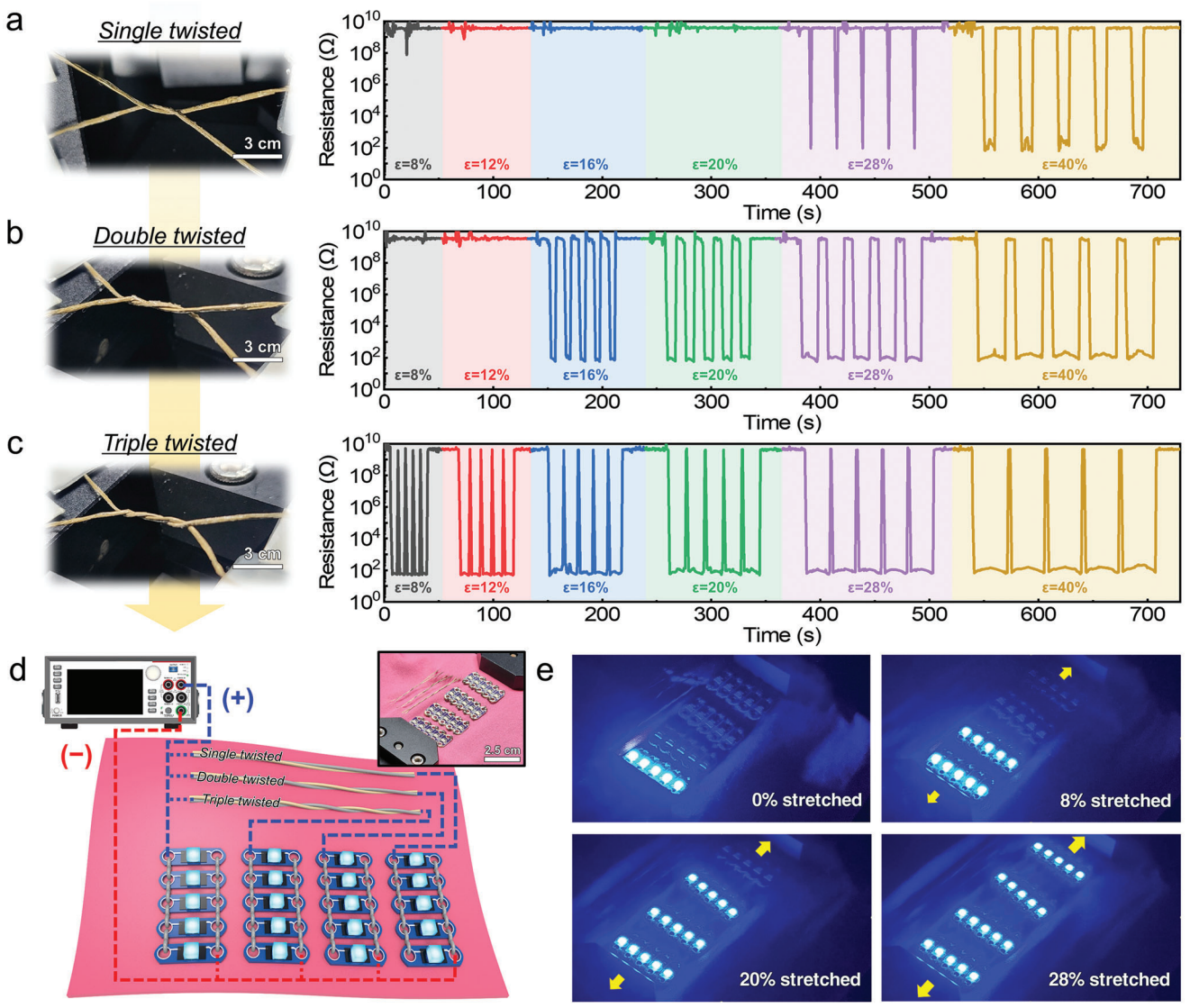

Figure 4. Sensitivity measurement results of the NRS fiber strain-sensors adjusted by the number of fiber twists and their visual demonstration. a–c) Electrical resistance variation under 5 cyclic stretching–releasing tests from 8% to 40% tensile strain of single twisted (a), double twisted (b), and triple twisted (c) NRS strain-sensors. d) 5 × 4 LED array with the NRS fiber strain-sensors in which the number of illuminated LEDs varies according to the degree of tensile strain, along with an inset photograph of the array. e) Photographs of fabricated 5 × 4 LED array operating according to different degree of tensile strain: 0% stretched, 8% stretched, 20% stretched, and 28% stretched.

In Equation (1), R_c represents the contact resistance of two contacted bodies and ρ and H are the resistivity and hardness of the bodies, respectively, assuming that the two bodies are composed of identical materials. n represents the number of contacting points within the contact area (in macroscale, the contact surface is actually composed of many individual contact points). P is the contact pressure applied and π is a constant parameter. Equation (1) shows that the contact resistance is in inverse proportion to contact pressure P and contact point n. With an increase in contact number n and contact pressure P, the contact resistance will decrease accordingly.

As used herein, the FEA simulations using the static structural module of the ANSYS workbench computational simulation were conducted to analyze the cause of the contact resistance change in strain-sensitivity depending on the number of twists. For the twisted fibers without an encapsulation layer, as can be seen in Figure S15a (Supporting Information), it depicts the equivalent elastic strain distribution analysis results when the triple-, double-, and single-twisted fibers were stretched by 20%. Similar to all three twisted fibers, the strain is applied across the entire fiber, with a higher concentration at the parallel contact points. To quantitatively analyze the cause of changes in the minimum tensile strain, which lowers the resistance due to contact between the two conductive fibers according to the number of twists, the contact area and contact pressure of the three structures were analyzed as per the tensile strain. As a result, in Figure S15b (Supporting Information), the contact area in the triple-twisted structure was ≈1.6 times that of the single-twisted

structure under a 20% strain condition. Similarly, in the case of contact pressure Figure S15c (Supporting Information), the triple-twisted structure showed ≈2.1 times greater pressure compared to the single-twisted structure under a 20% strain condition. This is because compressive stress perpendicular to the tensile stress direction mostly occurs at the crossing point during stretching. Consequently, as the number of twists increased, the contact pressure and contact area applied to the two fibers also increased, and the contact resistance could be reduced, in accordance with the previously mentioned Holm theory.

Similar trends were observed in the simulations with uniform crack-based SU-8 encapsulation layers on the NRS fiber strain-sensors. As seen in Figure S16a (Supporting Information), the equivalent elastic strain distribution for fibers without an encapsulation layer among the two twisted fibers resembles that of Figure S15a (Supporting Information), with strain distributed across the entire fiber. In contrast, the remaining fibers with an SU-8 encapsulation layer show minimal strain on the rigid SU-8 regions, while the cracked regions experience a higher strain, up to 80%, even when the overall fiber strain is only 20%. This observation suggests that the encapsulation layer with uniform cracks helps to distribute the strain more evenly across the fiber, preventing localized stress concentrations that could lead to premature failure. Additionally, similar to the fibers without an encapsulation layer, the contact area and contact pressure distribution of twisted fibers with an SU-8 encapsulation layer in Figure S16b,c (Supporting Information) increase with a higher number of twists for these sensors. In practical situations involving SU-8 encapsulated fibers, crack initiation and propagation occur at the crossing points of the twisted fibers due to stress concentration and increased contact pressure.[41] As a result, when there are more twists in the fibers, a greater number of cracks can be generated. This causes the more twisted structure to exhibit a dramatic change in resistance at a lower tensile strain compared to the less twisted structure.

For their visual demonstration, we developed 5 × 4 LED arrays with sewable LEDs in which the number of illuminated LEDs varies according to the degree of tensile strain. As shown in Figure 4d, every LED on the piece of highly stretchy spandex fabric was vertically connected by the fabricated AgNP/PU-based conductive fibers. Subsequently, the LEDs in the first vertical row were directly connected to the power supply so that they could be turned on all the time. Meanwhile, the second, third, and fourth rows of LEDs were connected to the power supply through triple-twisted, double-twisted, and single-twisted NRS fiber strain-sensors, respectively. Because NRS fiber strain-sensors with different sensitivities to strain were connected to the power supply, each connected row was designed to turn on in sequential response to 8%, 20%, and 28% tensile strain. As shown in Figure 4e, the operating results are consistent with the variation in the measured electrical resistance with the tensile strain for the three types of twisted NRS fiber strain-sensors. In addition, Video S1 (Supporting Information) shows a real-time image of the LED arrays, demonstrating that the number of illuminated LEDs increases as they are stretched up to 30% and returns to their original form when strain is removed. This video confirms that the performance of the LED arrays, which are sequentially turned on according to tensile strain, did not degrade even when deformation was repeated five times.

For another promising application with this strain-dependent LED on/off switching technology, we designed a stretchable display on fabric without lowering the image quality even under biaxial tensile strain conditions. Conventionally, stretchable displays exhibit a critical drawback related to the deterioration of image quality due to the increase in space between each pixel during mechanical stretching.[43] The degradation of display quality occurs as the resolution (the number of pixels per unit area) and luminance (the brightness per unit area) decrease, resulting in image distortion or blurring. To maintain the display's resolution and luminance per unit area before and after stretching, some researchers have introduced a novel design concept called "hidden-pixel" structures.[44,45] These structures incorporate some hidden-pixels that can be activated only when the distance between the normal-pixels increases under the tensile strain to sustain the initial pixel density.

To implement this hidden-pixel design concept on a textile-based wearable display, as depicted in **Figure 5**a, we grafted our developed negatively strain-resistive LED switching technology for additional demonstrative application. Depending on how the fabricated NRS fiber strain-sensors are introduced into each interconnect wiring the LED and power supply, the fabricated passive-matrix 5 × 5 LED display could realize hidden-pixels that only turned on when stretched in the *X*-axis, *Y*-axis, and biaxial directions. For this, anodes of all the LEDs were connected to the common anode of the power supply by stitching them vertically to the fabric, and cathodes of all the LEDs were connected horizontally to the common cathode of the power supply. Specifically, in the case of nine normal-pixels (see Figure 5b) that are always turned-on regardless of the tensile strain, they were connected directly to the power supply via the manufactured AgNP/PU-based conductive fibers without the NRS fiber strain-sensors. If the conductive fibers are used for this interconnect, no significant resistance occurred up to a 30% stretch; thus, the LED's luminosity was not significantly diminished even after stretching. In contrast, the anodes of the LEDs in the second and fourth horizontal rows were connected to the common anode through the X-axis NRS fiber strain-sensors, and the cathodes of the LEDs in the second and fourth vertical rows were connected to the common cathode through the Y-axis NRS fiber strain-sensors. As depicted in the circuit schematic diagram in Figure 5c, the nine black-marked LEDs are normal-pixels, while the six blue-marked LEDs and six red-marked LEDs are hidden-pixels that are only turned on after stretching in the X-axis and Y-axis directions, respectively. Additionally, in the case of the four yellow-marked LEDs, both the anode and cathode are connected to the NRS fiber strain-sensors, so both axes must be stretched to turn on the yellow-marked LEDs.

As shown in the result in Figure 5d and Video S2 (Supporting Information), the hidden-pixels are respectively switched on and off according to tensile strain applied along the *X*- and/or *Y*-axis directions in accordance with the logic flow previously described. By appropriately designing the triggering strain-sensor threshold, the increased pixel-to-pixel distance and, thus, the degradation of resolution under the tensile strain can be compensated for by selectively turning on hidden-pixels, and thus, the array's original resolution can be maintained. Although we demonstrated a conceptual resolution-maintenance process with the 5 × 5 low-resolution displays with 16 hidden-pixels in this study, we believe

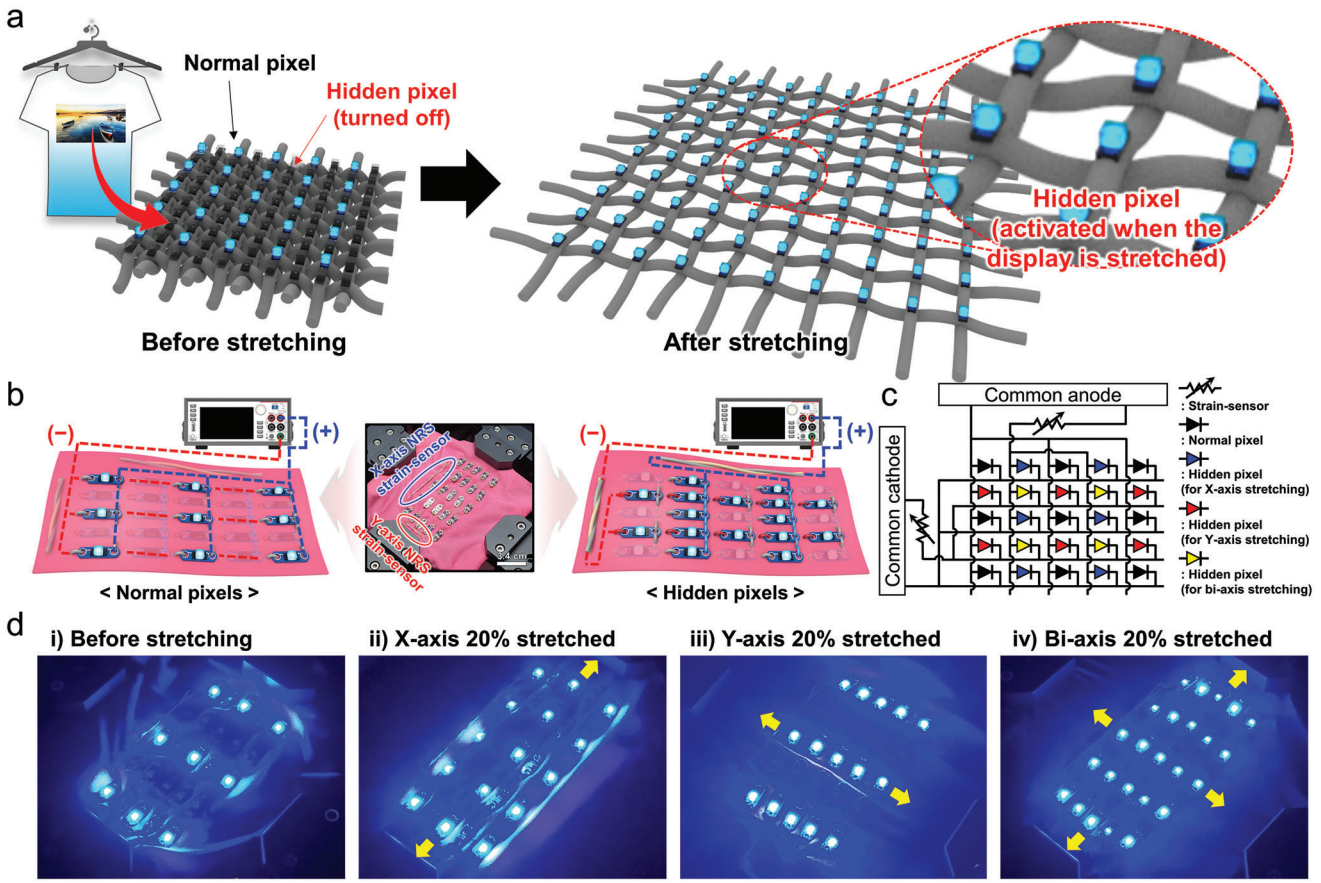

Figure 5. Systematic design and operation of a biaxially stretchable 5 × 5 LED display with the NRS fiber strain-sensors with hidden-pixel structures. a) Schematic diagram of textile-based stretchable displays with hidden pixel structure, and b) a fabricated 5 × 5 LED array with the NRS fiber strain-sensors, along with an inset photograph of the array. c) Equivalent circuit of the manufactured 5 × 5 LED array. d) Photographs of fabricated 5 × 5 LED array operating in accordance with each tensile strain: before stretching, *X*-axis 20% stretched, *Y*-axis 20% stretched, and biaxially 20% stretched.

that the same strategy can be incorporated into high-resolution wearable displays.

2.4. Application to Wearable Healthcare Monitoring Systems with Near-Zero Standby Power

To demonstrate the potential applications of their negatively strain-resistive switch behavior, we fabricated three actual clothing-based healthcare monitoring systems with near-zero standby power consumption using the NRS fiber strain-sensors. The extremely high resistivity in the sensing region contributed to an almost zero-current draft across the device before stretching, indicating that the power consumption in the standby-mode in the absence of strain could be reduced. This power-saving capability makes the NRS fiber strain-sensors ideally suited for a long-term strain monitor on massive infrastructure, which is driven only when a wearable device is worn by the user or when user movement is detected.

As the first practical application of our fabricated NRS fiber strain-sensors, we have developed a unique wearable healthcare monitoring system called "E-fitness pants". This monitoring system allows for a comparison of energy consumption between conventional P-GF sensors and our N-GF sensors. Designed to monitor various physical activities such as squats, lunges, and step-ups, the E-fitness pants can also count the repetitions, offering a comprehensive solution for fitness tracking and health monitoring. As shown in **Figure 6**a, the E-fitness pants incorporate strain sensors into both knees; The right knee uses our NRS fiber strain-sensor with a negative gauge factor (N-GF), while the left knee uses a single fiber sensor with a positive gauge factor (P-GF), based on our previous research.[12] This design allows us to compare the resistance change and power consumption of both strain-sensors during the same activity. In addition to measuring real-time power consumption, a sewable LED was affixed to the end of each sensor, allowing for intuitive observation of current flow and power consumption through changes in LED brightness. To ensure an accurate power comparison, we used strain sensors with similar resistances at ≈10–20% strain.

Each movement can be outlined as follows: Squat movements involve bending both knees simultaneously while maintaining a straight back and lowering the hips as if sitting in an imaginary chair. Lunge movements require stepping forward with one foot and bending both knees at a 90-degree angle, with the rear knee hovering above the ground and alternating between legs, which causes both knees to bend in each movement. Step-up

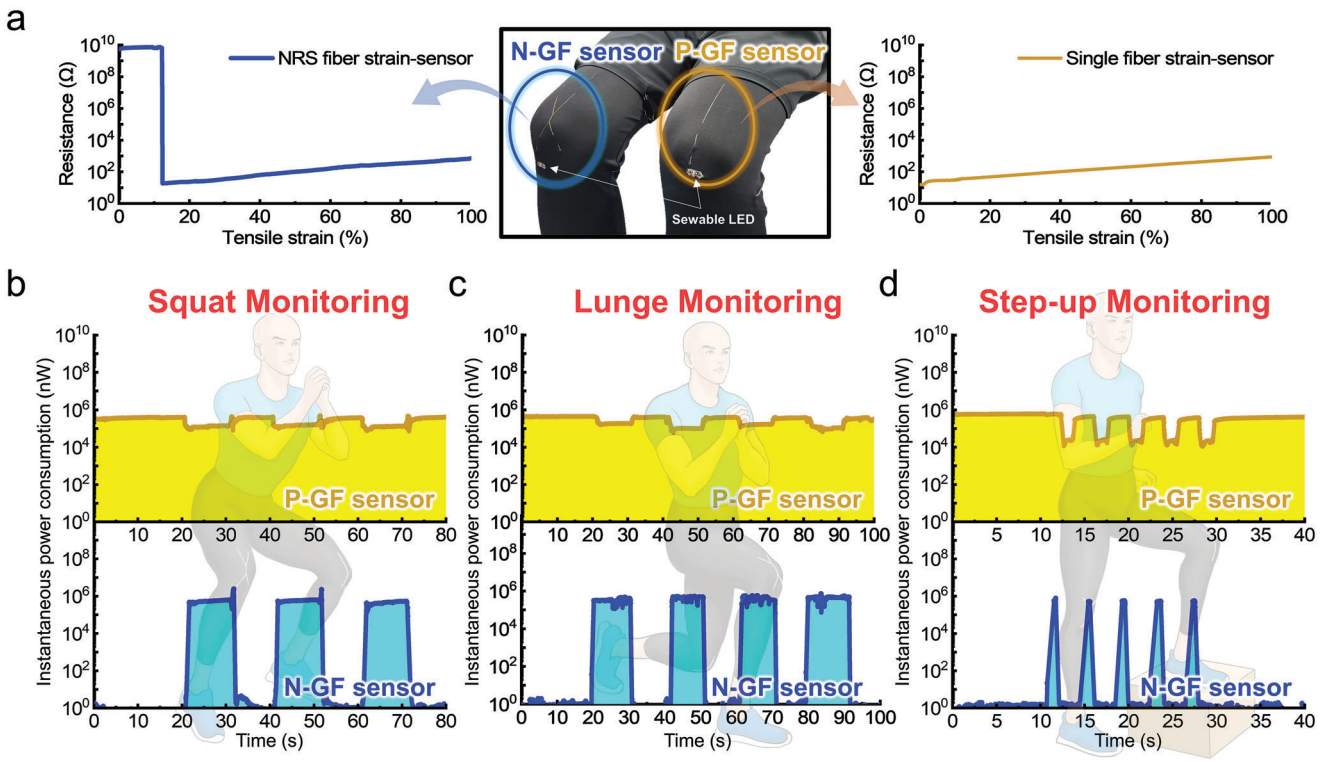

Figure 6. E-fitness pants for real-time tracking and exercise repetition counting. a) Photographs of the custom-designed E-fitness pants with the performance of distinct sensors inserted into the left and right knees. b) The instantaneous power consumption during squats, lunges, and step-ups, as monitored over time.

movements involve stepping up onto an elevated platform with one foot, bending the knee, then stepping back down and repeating with the opposite leg. At this time, the legs move one by one, so the knees also alternately bend one by one. These distinct knee strain patterns enable us to differentiate between various physical activities, as shown in Figure 6b.

As a result, the inserted P-GF sensor in the left knee continuously consumes over 10^5 nW due to its low resistance (below 100 Ω), whereas the inserted N-GF sensor in the right knee exhibits an initial resistance higher than 10^9 Ω, preventing current flow and resulting in near-zero standby power consumption. Therefore, power consumption was found to occur only during exercise activities in the right knee with the N-GF sensor connected. Moreover, by integrating the area of the graph, we observe a reduction of ≈29% in power consumption for squats, ≈48% for lunges, and ≈88% for step-ups when using N-GF sensors compared to P-GF sensors. These findings are evident in Figure 6b, which displays the instantaneous power consumption graph, and in Video S3 (Supporting Information), which shows the brightness changes in LEDs connected to each sensor. In more detail, according to the photographs in Figure S17 (Supporting Information) of each movement, the LED of the right knee, where the N-GF sensor is installed is not illuminated in the standby-mode; rather, the LED is only illuminated when the knee is stretched. In contrast, in the case of the left knee where the P-GF sensor is installed, the LED is continuously illuminated even without any movement, and when the knee is stretched, the resistance of the fiber increases and the LED brightness decreases. As demonstrated by this graph, LED brightness and power consumption are correlated, confirming that the near-zero standby power consumption of the N-GF sensors offers significant advantages in monitoring physical activities in a more energy-efficient manner.

Expanding upon merely counting exercise repetitions, the distinct characteristics of the NRS fiber strain-sensor we developed can be further utilized for additional applications. As seen in Figure S18 (Supporting Information), when stretched up to 100%, the NRS fiber strain-sensor exhibits a unique bidirectional characteristic, transitioning to an on-state with negative switching and subsequently displaying P-GF properties. Therefore, by leveraging this sensor, it can serve as both a simple on/off switch and a general strain-sensor in smart monitoring systems that operate only when a certain level of strain occurs after transitioning to the on-state. Such systems are energy-efficient, as they are only activated to precisely record quantitative strain in situations of excessive load or sudden changes.

By incorporating these unique switching characteristics into the previously developed E-fitness pants, we demonstrate that our device can be utilized for more than just counting the number of squats; it can also analyze the consistency and accuracy of these exercises. By calculating the rate of resistance increase after the rapid drop, we can determine whether each posture is maintained at a constant level and whether the user is performing the exercise correctly. As shown in Figure S19a (Supporting Information), the proper squat posture involves bending the knees to about a 90-degree angle while keeping the torso upright. In contrast, an improper squat posture might involve excessively

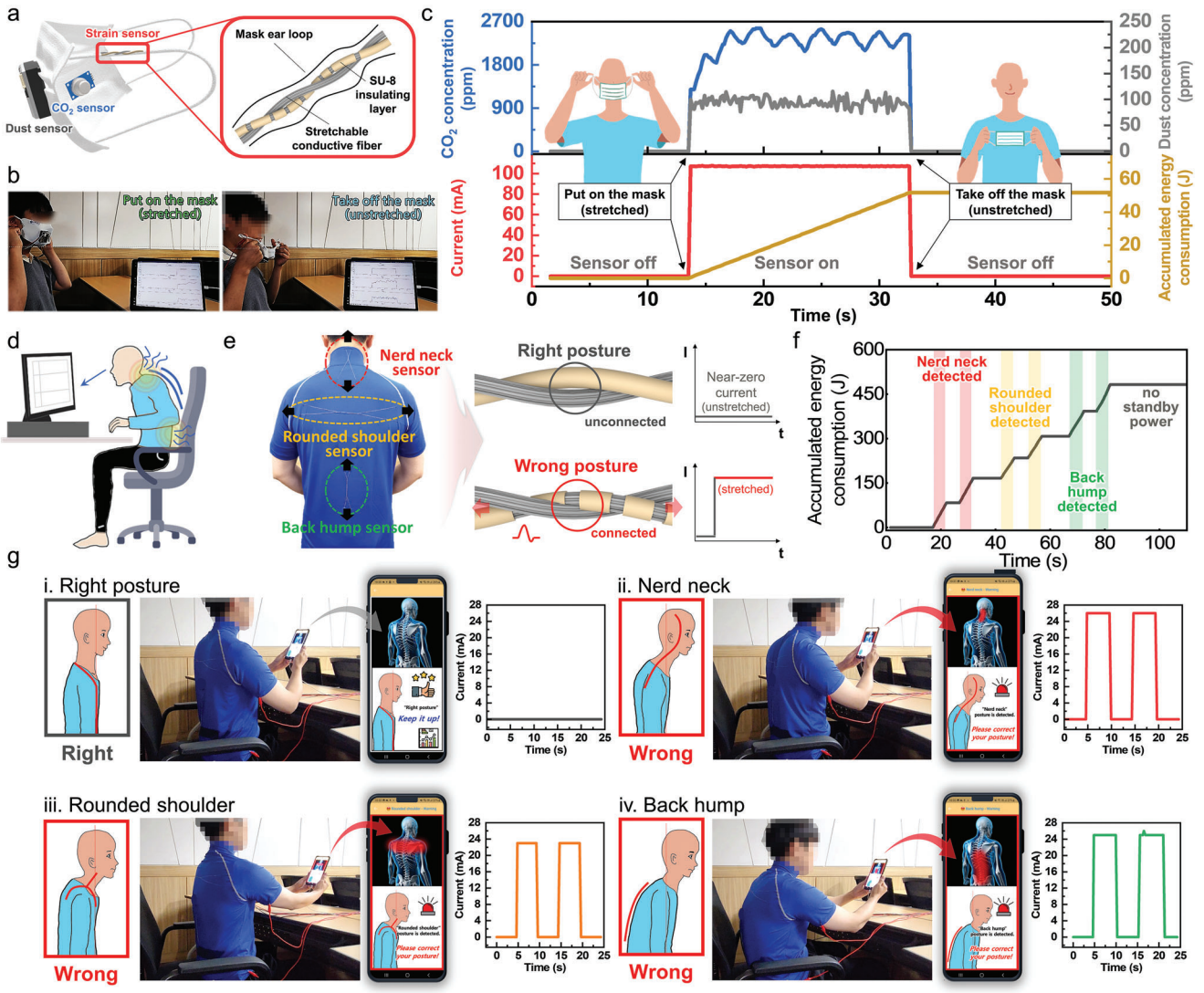

Figure 7. Practical demonstration of wearable healthcare monitoring systems based on the fabricated NRS fiber strain-sensors: smart-masks and posture-correction T-shirts. a) A schematic diagram of the fabricated smart-mask system. b) Photographs of the user before and after wearing the smart-mask. c) Measurement results of CO_2 and fine dust sensors using the smart-mask. d,e) Schematic diagrams of an example wrong posture (d) and the fabricated posture-correction T-shirts (e). f) Accumulated energy consumption according to each posture change. g) Real-time photographs and corresponding current measurement results of operated posture-correction T-shirts and the customized smartphone application for each posture.

bending the knees or not bending them enough, resulting in an unbalanced and potentially harmful position. Our proposed system effectively detects such issues using the NRS fiber strain-sensor embedded in the knee and provides feedback to the user. As illustrated in Figure S19b,c (Supporting Information), of the six squat repetitions, only the three that exhibit the switching characteristic are counted as valid squats. In cases like the second repetition, where the sensor in the knee is excessively stretched and displays P-GF characteristics, an "overextended" warning is issued. When the resistance value of the sensor is unstable, as in the third repetition, an "unstable posture" warning is provided. In situations like the fifth repetition, where the squat is performed but the knee does not stretch enough to cause a resistance change and reach the threshold, it is classified as an "insufficient angle" and not counted. This squat movement monitoring system can provide real-time feedback on exercise performance and accuracy while simultaneously demonstrating the advantages of the unique switching characteristics and linear resistance changes in response to strain.

Second, in order to further capitalize on the power-saving potential of the N-GF fiber strain-sensors, we developed an ultralow power smart-mask platform that could operate built-in sensors only when wearing the mask. Featuring a dust sensor on the exterior and a CO_2 gas sensor on the interior, this smart-mask, as depicted in **Figure 7**a, was configured to monitor the concentration of external fine dust and the user's breathing condition. All sensors, however, can only operate when the mask is worn over the ear loop because they are connected to the fabricated NRS fiber strain-sensors sewn onto the rubber band strap, which are only powered when the mask strap is stretched. In other words,

we developed a smart-mask-based platform with near-zero power consumption by appropriately customizing the sensitivity of the NRS fiber strain-sensors for the user to measure the concentration of fine dust and CO_2 only when the mask is worn, and both sensors do not operate when the mask is taken off, as shown in Figure 7b. The circuit block diagram of the system along with its interconnections is represented in Figure S20a (Supporting Information). The main electronic components of the conditioning circuitry include a microcontroller unit for control and data processing purposes and a current/power monitor for the CO_2 and dust sensors, which are connected only through the NRS fiber strain-sensors.

The results shown in Figure 7c and Video S4 (Supporting Information) confirm that there is no current flowing through the CO_2 and dust sensors during the initial 14 s when the user is not wearing the mask; thus, nothing is measured at all. Though, as soon as the user pulls the mask's rubber band strap and puts on the mask, current flows through the CO_2 and dust sensors, so that power is consumed while the two sensors detect the user's exhalation and outside dust normally. When the user took off the mask at ≈33 s, we found that even if the user breathed into the sensor, it could not be measured at all, and the two sensors were already turned off. In this instance, the current flowing through the sensor decreases to nearly 0 A; thus, no electrical energy is consumed. Consequently, by introducing the fabricated NRS fiber strain-sensors for their interconnect, a smart-mask-based real-time low-power monitoring system with near-zero standby power could be successfully implemented, which can have wide scalability through the application of various biosensors that detect physiological signals.

For the second practical application with the fabricated NRS fiber strain-sensors which accurately distinguish different mechanical stimuli by adjustable sensitivity, we applied the NRS fiber strain-sensors for posture correction T-shirt-based low-power monitoring systems that operate only when the user has the wrong posture. This is a platform designed as a part of the rehabilitation treatment for postural dysfunction, which has recently been dubbed a representative modern-day chronic disease. As shown in Figure 7d, as increasing office workers use computers for a long time and as mobile devices such as smartphones and tablet PCs become popular, there are numerous cases nowadays in which the resulting slouched posture causes deformation of the spine and joints, leading to chronic pain.[46] This is because inappropriate postures or habits are repeatedly adopted without awareness in daily and work life, causing the body's balance to be disturbed. If this broken body is neglected for a long time, it will eventually become a chronic condition that causes various types of pain.[47]

To prevent chronic diseases caused by improper posture, we developed a smart T-shirt-based monitoring system that can recognize and correct poor posture by displaying a pop-up alert on the user's mobile phone whenever their posture is incorrect. To achieve this, we placed the fabricated NRS fiber strain-sensors on the user's neck, shoulder, and spine with different sensitivities to detect three representative poor postures: "nerd-neck", rounded shoulder, and back hump. As shown in Figure 7e, when the NRS fiber strain-sensors were arranged in the three regions, a low-power posture monitoring system can be implemented based on the principle that current cannot flow to the sensors in the correct posture but can flow between the generated cracks when the sensors are stretched. To efficiently detect various postures by strategically positioning the sensors, we carried out an optimization process for the installation position and fiber length, as illustrated in Figure S21 (Supporting Information) as an example. Detailed optimization information can be found in the Supporting Information. After the optimization process, we designed and fabricated the monitoring system, which offered improved accuracy in detecting posture changes while providing real-time feedback to the user and supporting healthier posture habits.

The results in Figure 7f indicated that the developed device was an ultralow power monitoring system in which power is almost never consumed in the right posture, but power is consumed when current flows through the NRS fiber strain-sensors only in the wrong posture. Figure 7g displays the records of customized smartphone application screenshots as well as the measurement result of current flow through the entire circuit for each correct and incorrect posture. Because none of the three strain-sensors were stretched into the correct position, they all operated as open circuits with a current of 0 mA. When the posture changes to nerd-neck, rounded shoulder, and back hump, however, the strain-sensors on the neck, shoulder, and spine are stretched, and currents of ≈26, 23.5, and 24.5 mA flow through the entire circuit, respectively. In this regard, we could find that the screen of the smartphone varies appropriately by recognizing the body part of the stretched strain-sensors, clarifying that application development was impactful, in which the users could be alerted through notification that their posture was wrong. Notably, when designing the customized smartphone application, the back hump was given the highest priority because, depending on the posture, a rounded shoulder and a nerd-neck could also occur simultaneously. The details of the real-time monitoring and feedback using the smartphone are displayed in Video S5 (Supporting Information), and the circuit block diagram of the system is shown in Figure S20b (Supporting Information). Furthermore, screen captures of the developed smartphone application in the video can be seen in Figure S22 (Supporting Information). As such, we demonstrated that the NRS fiber strain-sensors can function as a mechanical-electric switch that can turn the power on/off in response to the strain in various wearable healthcare monitoring systems. Importantly, as they could apply the desired sensitivity by adjusting the number and length of fiber twisting, it can be utilized as interconnect with customized N-GF characteristics by simply sewing it to any fabric-type wearable device or clothes.

3. Conclusion

Twisted conductive-fiber-based NRS strain-sensors have been developed, that exhibit a considerable change in their conductivity under applied mechanical strain by depositing an SU-8 insulating encapsulation layer on the conductive stretchable fibers and then carefully adjusting the density and size of the cracks through selective UV-irradiation. The fabricated NRS fiber strain-sensors show an extreme resistance change of $\approx 10^{10}$ to 18 Ω after stretching, from insulator to metallic properties, which is an on/off switch-like device whose strain acts as a gate. Additionally, their superior stabilities were secured even after more than 5000 tensile strain repetitions, and the sensitivity of the strain

response could be adjusted from 8% to 28% based on the number of times these two fibers were twisted. By effectively utilizing these reliable and controllable switching characteristics, fabric-based biaxial stretchable LED arrays with hidden-pixels activated only when stretched were successfully implemented. Moreover, three real-time fully functional clothing systems—E-fitness pants for movement tracking, a smart-mask for detecting fine dust and breathing, and a posture correction T-shirt—were developed with near-zero power consumption in standby-mode and signal generation occurring only during stretching. This work paves the way for future advancements in human-machine interface design by providing a precise mechanical deformation detection mechanism in an ultralow-power healthcare monitoring system for textile electronics.

4. Experimental Section

Fabrication of the SU-8 Encapsulated Single Stretchable Conductive Fibers: The AgNP/PU-based stretchable conductive fibers were synthesized using a previously reported method.[12] Commercially available polyurethane-based stretchable fibers ≈500 µm-thick, Creora, were purchased from the Hyosung group and cleaned for 5 min in deionized (DI) water. To absorb the Ag^+ ions into the fibers, the stretchable fibers were submerged for 30 min into an Ag-precursor solution, comprising an ethanol solution with 35 wt% of $AgCF_3COO$ dissolved. After evaporating the ethanol solvent for 5 min, a 1:1 volume mixture of hydrazine hydrate and ethanol was dropped onto the fibers to convert the Ag^+ ions absorbed within the fibers into Ag nanoparticles. After 5 min, fibers were repeatedly rinsed with DI water to remove hydrazine hydrate, followed by air drying to eliminate any reduction agent. To achieve high fiber conductivity, the Ag nanoparticle reduction process was repeatedly performed. Then, the SU-8 2010 photoresist was used to encapsulate the conductive fibers by dipping methods. The fibers were heated at 85 °C for 10 min for pre-backing and were cured by selective UV irradiation (wavelength of 185 and 254 nm) for 2 h with customized shadow mask. To design the customized shadow mask, a flexible mask with sputtered Cr/Ag layers was fabricated on a poly(ethylene terephthalate) (PET) substrate, allowing it to conform to the fiber's cylindrical shape and minimize diffraction effects. This method could induce a difference in Young's moduli of the UV-irradiated and non-irradiated regions, forming uniform cracks as desired.

Fabrication and Device Characterization of the NRS fiber Strain-Sensors: The fabricated pristine AgNP/PU-based conductive fiber and the SU-8 encapsulated fiber thereon were twisted along the same length (5 cm) with different turns (180°, 360°, 540°) according to the desired sensor sensitivity and fixed to a stretchable fabric. Subsequently, custom-made 4-axis automatic stretching stages (Sciencetown, ST1) and a parameter analyzer (model 4200A; Keithley Instruments) were used to measure their electrical characteristics with a constant current of 0.1 mA under various strains on the device. Furthermore, a B2901A source meter (Keysight Technologies, USA) and an S2M force transducer (HBM, USA) were used to investigate the mechanical and electrical properties of the conductive fibers. A 7610F-Plus field-emission scanning electron microscope (JEOL, Japan) coupled with an EDS system was used to examine the surface morphologies and obtain cross-sectional images of the stretchable conductive fibers. The Young's modulus of SU-8 films before and after UV curing was measured by the nanoindentation system (TI-950, Bruker). For equivalent stress (von Mises) distribution analysis, the static structural and explicit dynamics module of a 3D ANSYS simulation tool was used.

Fabrication of the Electrospun PU-Nanofiber-Based Passivation Layer: A polyurethane solution for the electrospinning fabrication process was prepared to create a stretchable passivation layer on NRS fiber strain-sensors. PU (UR306300, Polyurethane-Granule-PU, purchased from GoodFellow) was dissolved in a 1:3 ratio of a mixed solution of N, N-Dimethylformamide (DMF) and tetrahydrofuran (THF) to form a 16 wt% PU solution. The prepared PU solution was thoroughly mixed at 80 °C by stirring for more than 5 h. The electrospinning (ESR100D, NanoNC) was performed at room temperature (24–26 °C) while maintaining humidity below 30%. The flow rate of the electrospinning process for the PU solution from a plastic syringe was fixed at 0.3 mL h^{-1}. The developed PU solution was electrospun onto an Al foil sheet substrate using a 23-gauge (23G) metallic needle, with a distance of 10 cm between the tip and substrate. After depositing the electrospun PU nanofibers on the substrate for 1 h, the fabricated NRS fiber strain-sensor was placed on the electrospun PU-nanofiber-based substrate. The electrospinning process was resumed, and the PU solution was electrospun onto the NRS fiber strain-sensor mounted substrate for an additional hour. Upon detaching the Al foil substrate, the electrospun PU nanofiber passivation layers for the NRS fiber strain-sensor were successfully fabricated.

Passive Matrix (PM) LED Arrays on Fabric with Hidden-Pixels: By appropriately adjusting the sensitivity of the NRS fiber strain-sensors fabricated above, two-types of PM LED arrays were fabricated on stretchable fabric using sewable LED sequins (LilyPad LEDs). First, 5 × 4 LED arrays were designed, in which the number of illuminated LEDs varied depending on the degree of fabric stretching, and the five LEDs were connected in a vertical line. For each row, the (+) electrode of the LEDs was connected to single-twisted, double-twisted, triple-twisted, and untwisted fibers, and the (−) electrode was commonly connected to a conductive fiber. Second, 5 × 5 LED arrays were designed in which the number of LEDs that are turned on varied depending on the *X*-axis and *Y*-axis stretching, as well as the biaxis stretching, and a hidden-pixel concept was introduced. The strain-sensors manufactured above were horizontally inserted in the *X*-axis direction and vertically in the *Y*-axis direction, respectively, on the upper and left sides of the LED array. Accordingly, the (+) electrode of the LEDs connected to the hidden-pixel was connected to the *X*-axis NRS fiber strain-sensor in a vertical line, and the (−) electrode was connected to the *Y*-axis NRS fiber strain-sensor in a horizontal line. The LEDs connected to the normal-pixel were directly connected to the power supply through conductive fibers without going through NRS fiber strain-sensors. In both LED arrays, the LED arrays were operated simultaneously during stretching with custom-made 4-axis automatic stretching stages (Sciencetown, ST1) and a parameter analyzer (model 4200A; Keithley Instruments).

Wearable Healthcare Monitoring Systems (Smart-Masks and Posture-Correction T-Shirts): In the case of smart-masks, a commercial dust concentration sensor (model GP2Y10; Sharp) and a dedicated adapter (model DFR028; DFROBOT) were attached to the outside, and a commercial gas sensor (model MQ-135; SMG) was attached to the inside. After connecting these two sensors in parallel, the NRS fiber strain-sensors fabricated between the two sensors and the power supply line were interconnected by sewing them together on the mask rubber band strap. Using this method, the power supply to the two sensors was designed to occur only when the mask strap stretched, i.e., when the user was wearing a mask. In addition, a bidirectional current/power monitor (model INA219; SMG) was inserted to measure the current and power flowing through the entire circuit, and the devices were operated by connecting the microcontroller board (model Uno Rev3; Arduino) and the Bluetooth module (model HC-06; SMG). In the case of posture correction T-shirts, three NRS strain-sensors with different sensitivity and length were sewn onto spandex T-shirts for detecting "nerd-neck", rounded shoulder, and back hump postures. The NRS strain-sensors were connected to the same microcontroller board and the Bluetooth module, and their resistance change according to their tensile strain was transmitted to the smartphone. Using this, a custom-developed smartphone application was designed to change the smartphone screen according to the resistance value of each sensor. Thus, all three NRS strain-sensors were open-circuits in correct posture, so the standby power consumption was near-zero, but each NRS strain-sensor was changed to a short-circuit in the wrong posture, resulting in power consumption in certain circumstances. The applicability of NRS strain-sensors was tested on volunteers who provided informed signed consent. Ethical approval was not required for this work.

Supporting Information

Supporting Information is available from the Wiley Online Library or from the author.

Acknowledgements

W.K.M. and C.W. contributed equally to this work. This research was supported by the National Research Foundation of Korea (NRF) Grant funded by the Korea Government (MSIT) (no. 2020M3H4A1A02084896). This work was also supported by the Priority Research Centers Program through the NRF (no. 2019R1A6A1A11055660) and ICONS (Institute of Convergence Science) at Yonsei University.

Conflict of Interest

The authors declare no conflict of interest.

Data Availability Statement

The data that support the findings of this study are available on request from the corresponding author. The data are not publicly available due to privacy or ethical restrictions.

Keywords

conductive fibers, monitoring systems, near-zero standby power, negative resistance switching, strain-sensors, wearable electronics

Received: April 17, 2023
Published online: July 19, 2023

[1] S. A. Musich, W. N. Burton, D. W. Edington, *Dis. Manage. Health Outcomes* **1999**, *5*, 153.
[2] Y. Ma, Y. Zhang, S. Cai, Z. Han, X. Liu, F. Wang, Y. Cao, Z. Wang, H. Li, Y. Chen, *Adv. Mater.* **2020**, *32*, 1902062.
[3] M. M. Baig, H. GholamHosseini, A. A. Moqeem, F. Mirza, M. Lindén, *J. Med. Syst.* **2017**, *41*, 115.
[4] L. Allet, R. H. Knols, K. Shirato, E. D. de Bruin, *Sensors* **2010**, *10*, 9026.
[5] R. Paradiso, L. Caldani, *Wearable Sensing and Intelligent Data Analysis for Respiratory Management*, (Eds: R. P. Paiva, P. de Carvalho, V. Kilintzis), Academic Press, Cambridge, UK **2022**.
[6] B. Lee, H. Cho, S. Jeong, J. Yoon, D. Jang, D. K. Lee, D. Kim, S. Chung, Y. Hong, *J. Inf. Disp.* **2022**, *23*, 163.
[7] V. Kaushik, J. Lee, J. Hong, S. Lee, S. Lee, J. Seo, C. Mahata, T. Lee, *Nanomaterials* **2015**, *5*, 1493.
[8] I. Wicaksono, C. I. Tucker, T. Sun, C. A. Guerrero, C. Liu, W. M. Woo, E. J. Pence, C. Dagdeviren, *npj Flexible Electron.* **2020**, *4*, 5.
[9] X. Lu, W. Shang, G. Chen, H. Wang, P. Tan, X. Deng, H. Song, Z. Xu, J. Huang, X. Zhou, *ACS Appl. Electron. Mater.* **2021**, *3*, 1477.
[10] C. Zhang, W. Fan, S. Wang, Q. Wang, Y. Zhang, K. Dong, *ACS Appl. Electron. Mater.* **2021**, *3*, 2449.
[11] A. Libanori, G. R. Chen, X. Zhao, Y. H. Zhou, J. Chen, *Nat. Electron.* **2022**, *5*, 142.
[12] J. Lee, S. Shin, S. Lee, J. Song, S. Kang, H. Han, S. Kim, S. Kim, J. Seo, D. Kim, T. Lee, *ACS Nano* **2018**, *12*, 4259.
[13] M. A. U. Khalid, S. H. Chang, *Compos. Struct.* **2022**, *284*, 115214.
[14] J. Woo, H. Lee, C. Yi, J. Lee, C. Won, S. Oh, J. Jekal, C. Kwon, S. Lee, J. Song, B. Choi, K. I. Jang, T. Lee, *Adv. Funct. Mater.* **2020**, *30*, 1910026.
[15] C. Won, S. Lee, H. H. Jung, J. Woo, K. Yoon, J. Lee, C. Kwon, M. Lee, H. Han, Y. Mei, K. I. Jang, T. Lee, *ACS Appl. Mater. Interfaces* **2020**, *12*, 45243.
[16] X. He, G. Shen, J. Liang, Z. Liu, Y. Xin, T. Liang, J. He, C. Zhang, Y. Chen, X. He, *ACS Appl. Electron. Mater.* **2021**, *3*, 3287.
[17] J. Lee, S. J. Ihle, G. S. Pellegrino, H. Kim, J. Yea, C. Y. Jeon, H. C. Son, C. Jin, D. Eberli, F. Schmid, B. L. Zambrano, A. F. Renz, C. Forro, H. Choi, K. I. Jang, R. Kung, J. Voros, *Nat. Electron.* **2021**, *4*, 291.
[18] J. Lee, B. Llerena Zambrano, J. Woo, K. Yoon, T. Lee, *Adv. Mater.* **2020**, *32*, 1902532.
[19] M. Kang, T.-W. Kim, *Appl. Sci.* **2021**, *11*, 6131.
[20] Y.-R. Ding, C.-H. Xue, X.-J. Guo, X. Wang, S.-T. Jia, Q.-F. An, *ACS Appl. Electron. Mater.* **2022**, *4*, 345.
[21] L. Li, Y. Zheng, E. Liu, X. Zhao, S. Yu, J. Wang, X. Han, F. Xu, Y. Cao, C. Lu, H. Gao, *Chem. Eng. J.* **2022**, *437*, 135399.
[22] X. Qu, Y. Wu, P. Ji, B. Wang, B. Wang, Q. Liang, Z. Han, J. Li, Z. Wu, S. Chen, G. Zhang, H. Wang, *ACS Appl. Mater. Interfaces* **2022**, *14*, 29167.
[23] F. Huang, J. Hu, X. Yan, *Textiles* **2022**, *2*, 81.
[24] D. Y. Park, D. J. Joe, D. H. Kim, H. Park, J. H. Han, C. K. Jeong, H. Park, J. G. Park, B. Joung, K. J. Lee, *Adv. Mater.* **2017**, *29*, 1702308.
[25] Y. G. Kim, J. H. Song, S. Hong, S. H. Ahn, *npj Flexible Electron.* **2022**, *6*, 52.
[26] S. Veeralingam, A. N. K. Ravindranath, S. Badhulika, *Adv. Mater. Interfaces* **2020**, *7*, 2000568.
[27] A. Risso, V. Rajaram, S. Kang, S. D. Calisgan, Z. Qian, M. Rinaldi, in *2021 21st Int. Conf. on Solid-State Sensors, Actuators and Microsystems (Transducers)*, IEEE, Piscataway, NJ, USA, **2021**, pp. 565–568.
[28] K. Zhao, W. Niu, S. Zhang, *J. Mater. Sci.* **2019**, *55*, 2439.
[29] W. Hong, C. Jiang, M. Qin, Z. Song, P. Ji, L. Wang, K. Tu, L. Lu, Z. Guo, B. Yang, *Sci. Adv.* **2021**, *7*, eabj4273.
[30] S. Chae, W. J. Choi, I. Fotev, E. Bittrich, P. Uhlmann, M. Schubert, D. Makarov, J. Wagner, A. Pashkin, A. Fery, *Adv. Mater.* **2021**, *33*, 2104769.
[31] A. J. Granero, P. Wagner, K. Wagner, J. M. Razal, G. G. Wallace, M. in het Panhuis, *Adv. Funct. Mater.* **2011**, *21*, 955.
[32] J. Eom, R. Jaisutti, H. Lee, W. Lee, J.-S. Heo, J.-Y. Lee, S. K. Park, Y.-H. Kim, *ACS Appl. Mater. Interfaces* **2017**, *9*, 10190.
[33] Y. Wang, Y. Su, Y. Zhang, M. Chen, *ACS Appl. Mater. Interfaces* **2022**, *14*, 5661.
[34] M. Zhang, M. Wang, M. Zhang, Q. Gao, X. Feng, Y. Zhang, J. Hu, G. Wu, *Org. Electron.* **2020**, *81*, 105677.
[35] H. Kim, T.-H. Kang, J. Ahn, H. Han, S. Park, S. J. Kim, M.-C. Park, S.-h. Paik, D. K. Hwang, H. Yi, J. A. Lim, *ACS Nano* **2020**, *14*, 17213.
[36] N. Luo, J. Zhang, X. Ding, Z. Zhou, Q. Zhang, Y.-T. Zhang, S.-C. Chen, J.-L. Hu, N. Zhao, *Adv. Mater. Technol.* **2018**, *3*, 1700222.
[37] S. Chung, S. Park, *J. Mech. Sci. Technol.* **2013**, *27*, 2701.
[38] D. Wu, Y. Jia, D. Liao, B. Zhang, C. Liu, N. Wang, W. Peng, L. Huang, *J. Inf. Disp.* **2022**, *24*, 93.
[39] H. Cho, B. Lee, D. Jang, J. Yoon, S. Chung, Y. Hong, *Mater. Horiz.* **2022**, *9*, 2053.
[40] Y. Lee, H. Cho, H. Yoon, H. Kang, H. Yoo, H. Zhou, S. Jeong, G. H. Lee, G. Kim, G.-T. Go, J. Seo, T.-W. Lee, Y. Hong, Y. Yun, *Adv. Mater. Technol.* **2023**, https://doi.org/10.1002/admt.202201067.
[41] S. Choi, K. Yoon, S. Lee, H. J. Lee, J. Lee, D. W. Kim, M. S. Kim, T. Lee, C. Pang, *Adv. Funct. Mater.* **2019**, *29*, 1905808.
[42] C. Zhang, W. Ren, X. Liao, *Materials* **2022**, *15*, 5667.
[43] S. Choi, S. Kim, H. Kim, B. Lee, T. Kim, Y. Hong, *IEEE Sens. J.* **2020**, *20*, 14655.
[44] Y. Lee, B. J. Kim, L. Hu, J. Hong, J.-H. Ahn, *Mater. Today* **2022**, *53*, 51.
[45] S. Kim, J. Byun, S. Choi, D. Kim, T. Kim, S. Chung, Y. Hong, *Adv. Mater.* **2014**, *26*, 3094.

[46] Y. Jiang, J. An, F. Liang, G. Y. Zuo, J. Yi, C. A. Ning, H. Zhang, K. Dong, Z. L. Wang, *Nano Res.* **2022**, *15*, 8389.

[47] R. Z. Lin, H. J. Kim, S. Achavananthadith, S. A. Kurt, S. C. C. Tan, H. C. Yao, B. C. K. Tee, J. K. W. Lee, J. S. Ho, *Nat. Commun.* **2020**, *11*, 444.